The Electrochemical Society
Advancing solid state & electrochemical science & technology

Tailoring Electrocatalytic Properties of Pt Nanoparticles Grown on Ti$_3$C$_2$T$_X$ MXene Surface

View the article online for updates and enhancements.

Tailoring Electrocatalytic Properties of Pt Nanoparticles Grown on Ti$_3$C$_2$T$_X$ MXene Surface

Jaroslav Filip,[1] Sifani Zavahir,[2] Lenka Lorencova,[3] Tomas Bertok,[3] Ammar Bin Yousaf,[2] Khaled A. Mahmoud,[4] Jan Tkac,[3] and Peter Kasak [2,z]

[1]*Department of Environmental Protection Engineering, Faculty of Technology, Tomas Bata University in Zlin, 760 01 Zlin, Czech Republic*
[2]*Center for Advanced Materials, Qatar University, 2713 Doha, Qatar*
[3]*Slovak Academy of Sciences, Institute of Chemistry, Department of Glycobiotechnology, 845 38 Bratislava, Slovak Republic*
[4]*Qatar Environment and Energy Research Institute (QEERI), Hamad Bin Khalifa University (HBKU), Doha, Qatar*

In this work, the spontaneous and NaBH$_4$-induced reduction of chloroplatinic acid on the surface of Ti$_3$C$_2$T$_X$ MXene was investigated to synthesize a hybrid PtNP-decorated MXene nanomaterial (MX-Pt) with potential as hydrogen evolution (HER) or oxygen reduction reaction (ORR) catalyst properties. The initial Pt concentration, reduction time and presence of additional reducing agents were varied, and as-synthesized nanocomposites were characterized thoroughly by XRD, EDX, SEM and XPS analysis and by electrochemical methods. Composites containing 14 wt% Pt showed HER with an onset potential of −75.9 mV and a current density of −10 mA cm^{-2} achieved at −226 mV. The spontaneous deposition of PtNPs on MXene improved the electrocatalytic properties over using an external reducing agent to form PtNP, which was explained based on the different rates of oxidation of Ti in the initial MXene support. Furthermore, good stability of the electrode modified by the MX-Pt was achieved without any polymeric binder and the HER reaction achieved only a negligible decrease over 3 000 potentiodynamic cycles.
© 2019 The Electrochemical Society. [DOI: 10.1149/2.0991902jes]

Ever-increasing energy consumption worldwide demands a continuous search for alternative energy sources to inefficient and unsustainable fossil fuel combustion. Hydrogen can be an alternative solution providing a renewable, high energy density fuel with practically zero emissions during combustion. Among other ways, hydrogen can be harnessed electrochemically via the "hydrogen evolution reaction" (HER), where water is electrolysed, H$^+$ moieties are reduced and, consequently, H$_2$ is released. Moreover, an affordable catalyst for the oxygen reduction reaction (ORR) for the O–O bond breaking is highly demanded since this reaction is part of the electrocatalytic process in fuel cells or lithium-air batteries. In real applications, different nanomaterials were tested as electrocatalysts of such reactions, including transition metal dichalcogenide-based surfaces (e.g., MoS$_2$) (see, for example Refs. 1–4), heteroatom-doped carbon nanomaterials[5–8] or metal nanoparticles, including Pt nanoparticles (PtNPs) - see for example Refs. 9–14 The latter has been employed in many modifications, including their in situ synthesis on diverse (nano)substrates via a spontaneous or assisted reduction of Pt ions.[15,16] The reduction process in such cases is governed either by the "oxidizability" of the substrate/support nanoparticles or by an external reducing agent.

MXene, a novel layered, 2D nanomaterial, was first synthesized and thoroughly characterized by Gogotsi's research team.[17] It is typically synthesized by Al leaching from initial "MAX" phase, where M represents metal ion (Ti, V, etc.), A represents interlayers of Al and X represents C or N atoms. After Al etching, layered Ti$_3$C$_2$T$_X$ MXene sheets are formed with surface modified with =O, -OH and -F groups (T$_X$ in Ti$_3$C$_2$T$_X$) - see for example Ref. 18 and the references therein. Because of good mechanical and electrical properties, MXenes can be used in energy transformation and storage applications,[19, 20] sensors[21,22] and biosensors.[23]

Some studies reported low suitability of titanium carbide MXenes for the HER.[24] On the other hand, high-performance in HER electrocatalysis[25] can be achieved by MXene-based nanoparticles coated with Au, Pd, Ag,[26] or Pt nanoparticles.[27] It was revealed that these modifications increased the catalytic properties of the prepared nanomaterial compared to initial ones, as well as their stability during electrochemical performance.[27] Synthesis of nanoparticles was achieved for example by reduction of metal salt by ethylene glycol[28] or from ethanolic dispersion.[29] Furthermore, PtNPs deposited on different kinds of (nanostructured) substrates are commonly used ORR catalysts in proton exchange membrane fuel cells[30] and direct methanol

fuel cells.[31] It should be also noted that ability of MXene nanosheets to spontaneously reduce Me^{n+} ions (namely Au, Pd, Ag) has been reported and employed for surface enhanced Raman scattering of the prepared MXene-nanoparticles nanohybrids.[26]

In this work, we adapted the abovementioned mechanisms to prepare PtNPs-decorated Ti$_3$C$_2$T$_X$ MXene (MX-Pt) hybrid nanostructures and investigate their electrocatalytic properties as well as some features of the synthesis process. The substrate material, i.e., Ti$_3$C$_2$T$_X$, is known to be oxidized by, for example, hydrogen peroxide.[32] This process is accompanied by changes in the structure of the initial MXene.[32] It can be anticipated that the application of an additional reducing agent for PtNPs synthesis may help to avoid such oxidative damage of Ti$_3$C$_2$T$_X$ MXene. Hence, two approaches were compared in this study; first, Ti$_3$C$_2$T$_X$ MXene was treated with a platinum precursor (hexachloroplatinic acid), and reduction to Pt nanoparticles proceeded on the MXene surface with a supposed partial oxidation of Ti in the MXene structure, leading to TiO$_2$ NP formation. In the second approach NaBH$_4$ was applied as a reducing agent in addition to the Pt precursor, as is depicted in Scheme 1. In addition to differences in chemical composition and particle arrangement revealed by conventional characterization methods (EDX, SEM, XPS, XRD), the catalytic properties of the prepared MX-Pt toward the HER and ORR were also tested electrochemically, and it was found that the HER catalysis and stability can be improved significantly upon simple conjugation of Ti$_3$C$_2$T$_X$ MXene with Pt nanoparticles in a lower amount than in conventional PtNP-based nanocatalysts.

Materials and Methods

Materials.—Ti$_3$AlC$_2$, LiF, H$_2$PtCl$_6$ and NaBH$_4$ were purchased from Sigma Aldrich. HCl conc. 37%, and absolute ethanol were purchased from ChemSupply. These chemicals were used as received without further purification. In all sample preparations and experiments deionized water (DW) was used.

Preparation of MXene.—Ti$_3$C$_2$T$_X$ MXene was synthesized by etching Ti$_3$AlC$_2$ LiF in HCl at 35°C for 24 h as in the previous literature.[25,33] It was then treated with probe sonication for 60 minutes (pulse sequence: 3 pulse-on, 1 pulse-off) at 750 kW of power with an amplitude of 80% in an ice bath and under a constant flow of nitrogen. This step is important to delaminate the Ti$_3$C$_2$T$_X$ layers. The solution was then separated by centrifugation at 3 000 rpm. The supernatant was collected and was freeze-dried to powder.

[z]E-mail: peter.kasak@qu.edu.qa
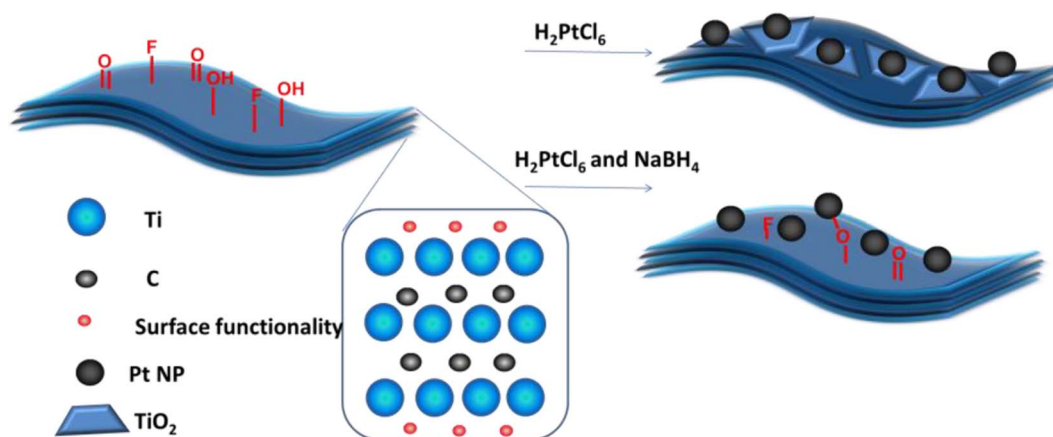
Scheme 1. Illustration of the $Ti_3C_2T_X$ MXene structure and its modification with Pt nanoparticles with and without employment of the reducing agent $NaBH_4$.

Synthesis of PtNPs on MXene.—Each batch was prepared in a separate 20 mL vial, which was loaded with 10 mg of as-synthesized dry $Ti_3C_2T_X$ MXene powder dispersed in 10 mL of DW by ultrasonication for 10 minutes. Then, 0.5 mL or 2.5 mL of 10 mg mL^{-1} of chloroplatinic acid stock solution (to prepare 5 wt% or 25 wt% Pt in the incubation solution, as is summarized in Table I) was added to the dispersion of MXene and DW, followed by ultrasonication for another 20 minutes. Four samples, namely, MX-Pt_1, MX-Pt_2, MX-Pt_3 and MX-Pt_4, were prepared by combining different concentrations of Pt with a certain incubation time (see Table I). The samples MX-Pt-RA_1 and MX-Pt-RA_2 with an external reducing agent were prepared in the same way, but with the addition of 10 μL aliquots of 10 mM ice-cold $NaBH_4$ immediately after mixing H_2PtCl_6 with MXene, followed by ultrasonication for 20 minutes (see Table I). All batch products were then separated by centrifugation at 12 000 rpm for 10 minutes, washed with absolute ethanol three times under centrifugation, and dried by the freeze drying technique.

Electrochemical measurements.—Electrochemical measurements were performed on a Gamry 3000 potentiostat with a Ag/AgCl/saturated KCl reference electrode, Pt wire as the counter electrode, and a modified disc glassy carbon electrode (GCE; geometric surface area of 0.07 cm^2; BASi, USA) as a working electrode. Electrolyte solutions of 100 mM H_2SO_4 and 100 mM NaOH were used accordingly under continuous gas purging: oxygen (in aeration) and nitrogen (in deaeration). Cyclic voltammograms (CVs) were performed at a scan rate of 50 mV s^{-1} in the potential ranges denoted in the text herein, unless stated otherwise. All potentials are expressed against a reversible hydrogen electrode (RHE). In addition to using a stationary electrode, experiment measurements were performed with a rotating disc electrode (RDE). In this case, a glassy carbon shaft electrode was modified with prepared MX-Pt hybrids mounted on a controllable rotor (Gamry RDE710) and potentiodynamic polarization curves were recorded with rotating speeds of 0, 500, 1 000, 1 500, 2 000 and 3 000 rpm. In all cases, the electrodes were modified by drop-casting 10 μL or 20 μL aliquots of an MX-Pt nanohybrid dispersion (0.5 mg mL^{-1} in DW, dispersed by 30 min ultra-sonication) on the surface of the GCE or RDE, respectively, and drying under reduced pressure at room temperature until the modified electrodes were dried. Furthermore, the modified RDE electrodes were employed for the Tafel slope determination employing linear scan voltammetry (LSV) measurements performed in deaerated 100 mM H_2SO_4 at a scan rate of 0.5 mV s^{-1}.

Surface characterization methods.—*Scanning electron microscopy (SEM).*— The SEM images of MX-Pt hybrids treated in the case of electrode modification were recorded using a Nova NanoSEM 450 (FEI, USA) microscope using an accelerated voltage of 3 kV. The composition was determined by energy dispersive X-ray spectroscopy (EDX; FEI Quanta 200 SEM equipped with an EDX microanalysis system, FEI, USA). Good resolution of the SEM images was ensured by a few nm Au layer sputter-coated on the samples.

X-ray photoelectron spectroscopy (XPS).—XPS signals were recorded using AXIS ULTRA DLD (Kratos Analytical Ltd, UK) system equipped with Al KαX-ray source. The spectra were acquired in constant analyser energy mode with a pass energy of 160 eV at 10 kV, and a 10 mA emission current for the survey. The individual scans were performed with a pass energy of 10 eV at 15 kV, and a 15 mA emission current. A spectral calibration was performed using the automated calibration routine and the internal C 1s standard. The surface compositions (in atomic %) were determined by considering the integrated peak areas of the detected atoms and the oxidative state using Origin software. The complex peaks were evaluated using the "multiple peak simulation" function of the Origin software with automatic parameters, and the GAUSSAMP fitting function, which was found to provide the best results in terms of the fitting correlation coefficient.

Table I. Specifications, reaction conditions and chemical composition of samples. RA - reducing agnt; t - incubation time; c_{INI} - initial concentration of Pt in the incubation solution; Pt/e - Pt load on single electrode.

Sample code	RA	t (h)	c_{INI} % (m/v)	atom %/weight %				Pt /e (μg)
				C	O	Ti	Pt	
MX	NA	NA	NA	10.63/4.56	50.46/28.85	38.92/66.59	0/0	0
MX-Pt_1	none	2	5	17.75/8.27	50.34/31.28	31.41/58.44	0.46/2.01	0.201
MX-Pt_2	none	24	5	16.86/7.93	54.01/34.22	28.93/54.86	0.39/2.99	0.299
MX-Pt_3	none	2	25	23.62/13.73	58.20/43.87	17.93/40.45	0.25/2.31	0.231
MX-Pt_4	none	24	25	15.02/6.32	53.26/30.02	29.29/49.14	2.12/14.54	1.454
MX-Pt-RA_1	NaBH$_4$	4	5	16.82/7.97	52.96/33.45	29.96/56.62	0.25/1.96	0.196
MX-Pt-RA_2	NaBH$_4$	4	25	20.08/11.21	60.55/45.01	19.27/42.86	0.1/0.92	0.092
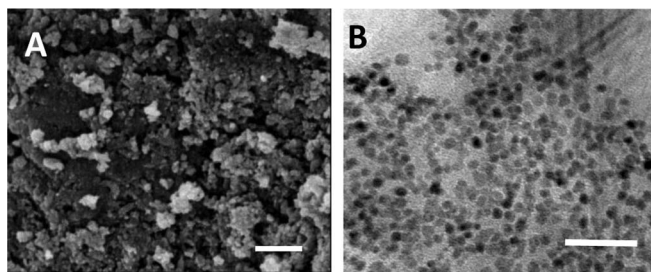
Figure 1. A) SEM and B) TEM images of MX-Pt_4 sample. Scale bar is 200 and 20 nm, respectively.

X-ray diffraction (XRD).—MX-Pt samples were characterized using XRD equipment Empyrean with irradiation source Cu Kα1 (0.15406 nm) at tension of 45 kV and current of 40 mA and detector PIXcel[1D] with stage platform with adjustable Z-height (all from PANalytical). Value of Z-height was determined for each sample using micrometer. X-ray diffraction was observed in gonio mode in 2θ range of 4°–80° with step size 0.0066° and scan speed 0.055° s⁻¹. Sample preparation method was the same as for the electrode modification, only glass slide was used as the support.

Results and Discussion

Spectroscopic and microscopic characterization of MX-Pt samples.—Different reaction times in combination with a reducing agent (RA) and the Pt precursor load in the incubation solutions were chosen to further investigate the influence of the preparation conditions on the final nanoparticles composition. The detailed composition obtained from EDX analysis and the preparation conditions are described in the experimental section and in Table I. EDX analyses were performed to assess the bulk composition of the prepared nanoparticles. Values in Table I confirmed that longer synthesis times as well as higher Pt precursor concentrations resulted in increased Pt content in the prepared MX-Pt hybrids. The EDX measurements also revealed a fundamental difference between the total Pt amount in the samples prepared with and without the RA. While the latter did not exceed 0.25 at.%, MX-Pt_2 and MX-Pt_4 exhibited 0.39 and 2.12 at.% Pt, respectively, which are significantly higher values. The higher values can be ascribed to the fact that, without the RA, the Pt precursors react directly with MXene moieties and, therefore, were stabilized faster on the MXene surface, which allowed for a higher yield. It should be noted that in in-situ synthesized PtNPs on $Ti_3C_2T_X$-based nanoparticles,[29] the EDX measurement revealed 16.94 at.% Pt, which is more than 6-fold higher than that for MX-Pt_4. Nevertheless, due to the difference in NP synthesis protocols, it is difficult to make a direct comparison of these values. Other papers reported the preparation of Pt-C particles with much higher Pt content (e.g., 74 wt% in the final catalyst powder – calculated,[34] or 60% reported in Ref. [35]). It is also known that many high-performance Pt-C catalysts contain approximately 20–60% Pt. It is, however, difficult to compare Pt-C directly with PtNPs synthesized on the MXene surface.

The morphology of the obtained heterostructures was also investigated by SEM. Small features were observed in the structure of composite MX-Pt_4 (Fig. 1A). The Pt nanoparticles were very well dispersed and densely covering the surface of MXene. Similar features were observed also in the MX-Pt-RA_2 sample prepared with the addition of a reducing agent confirming a certain level of PtNP growth. TEM of MX-Pt_4 revealed a homogeneous distribution of PtNPs (average diameter of 3 nm) on the surface of the MXene sheets (Fig. 1B). On this level of characterization, however, it is difficult to see any substantial difference.

EDX micromapping of the investigated surfaces has revealed a relatively homogeneous distribution of all surveyed elements without the formation of isolated aggregates (Fig. S1).

XRD was used to further elucidate the structural changes of the MXene structure. MX-Pt samples prepared without the reducing agent revealed peaks typical of MXene samples, i.e. broad peaks at approximately 6.4° and sharp peaks at 19.1°. All samples also exhibited sharp bifurcated peaks at 2θ angles of 38.8° and 38.9° attributed to the (111) crystal structure of Pt. Both the MX-Pt-RA_1 and MX-Pt-RA_2 samples prepared with the external reducing agent also exhibited the "MXene" peaks at 6.4°, small features at approximately 19.0° and, accordingly, a Pt111 bifurcated peak at 38.8° and 39.0° (see Fig. 2). The "MXene" peaks at the lowest 2θ values can be presumably assigned to exfoliated nanoparticles with the largest spacing between the individual $Ti_3C_2T_X$ layers. Interestingly, these peaks obviously diminished during the synthesis of PtNPs without the reducing agent; they were present only in the sample with the lowest Pt precursor concentration and with the shortest synthesis time (Fig. 2 and Table S1). Most probable explanation is that Ti-C bonds in $Ti_3C_2T_X$ surface layers are oxidized to produce TiO_2-like crystals/nanoparticles and amorphous carbon[36] as a result of Pt precursor reduction. TiO_2 formation probably destroys regular structures represented by the mentioned peaks at approximately 6.5–7°.[32] On the other hand, synthesis of PtNPs with the aid of the reducing agent obviously did not cause such strong oxidation of Ti-C in the original material, as deduced from the XRD peaks at 6.5° and 6.4° with absolute heights of 2 230 and 1 910 detected from MX-Pt-RA_1 and MX-Pt-RA_2, respectively (see Fig. 2 and Table S1). It can be suggested that use of the reducing agent helps to retain the structure of exfoliated MXene nanoparticles.[33]

The samples also exhibited peaks at 2θ = 19.5°, although with a very low intensity relative to the 6.5° and 9.5° peaks (Table S1). This demonstrates the possible closeness of the TiO_2 anatase (101) peak (25.2°[37,38]). Furthermore, the peak at approximately 19° is, according to some authors, assigned to titanium oxides,[39] while other authors assign this peak to titanium oxide-containing ceramics.[40] It can also be speculated that sub-stoichiometric oxidation of Ti occurred resulting in the creation of Magneli phases,[41] which may also reportedly provide XRD peaks at approximately 19°.[42–45] These structures, however, have been typically prepared by the thermal or thermochemical reduction of TiO_2. Involvement of Ti-C atoms in the formed structures is further supported by the fact that upon in situ synthesis of PtNPs on purely carbonaceous substrates (graphene, carbon nanotubes), only peaks assigned for Pt have emerged.[46,47] The XRD results are consistent with the hypothesis that these structures are formed predominantly without the use of a reducing agent, i.e., the reducing agent helps to efficiently retain the initial MXene structure. The presence of PtNPs was confirmed by a Pt111 peak at 2θ = 38.8°.[48] As expected, without the reducing agent, the highest peaks for the Pt111 crystals were detected with the use of 25% Pt precursor incubated for 24 hours and 2 hours (Fig. 2C), and samples MX-Pt_1 and MX-Pt_2 followed the pattern observed earlier for the "MXene" peak at 9.5°. The same pattern was observed for Pt111 peaks of RA samples, only they exhibited absolute heights much smaller than all MX-Pt samples without RA. Furthermore, the XRD peaks of the Pt_3Ti alloy have been reported to appear at approximately 2θ = 39°, overlapping with titanium oxides peaks.[44] From different patterns composed of Pt-related peaks of MX-Pt and MX-Pt-RA materials (Figs. 2C, 2D), it can be suggested that without the RA more Pt-Ti alloy particles are formed (the peak at the lower 2θ angle), while with an external reducing agent, the "alloy" peak is suppressed suggesting the formation of Pt nanoparticles. It can be concluded that without RA, the XRD patterns more closely resemble the original MXene spectra (data not shown). This resemblance is further supported by peaks at ~19.5°, while for both the initial MXene and MX-Pt-RA samples, this peak was almost negligible. Furthermore, it increased significantly for samples prepared without the RA.

It should be noted that Xie et al.[29] reported the in situ synthesis of PtNPs on $Ti_3C_2T_X$-based particles, without a reducing agent. Their XRD results suggest only a slight decrease in the MXene peak (9.5°) and emerging peaks for the 111, 200 and 220 conformations of Pt. Similarly, Satheeskumar et al. used a similar approach to modify $Ti_3C_2T_X$ MXene with Au, Pd and Ag NPs also without a reducing agent. No MXene peak decrease was mentioned.[26] Finally, it should
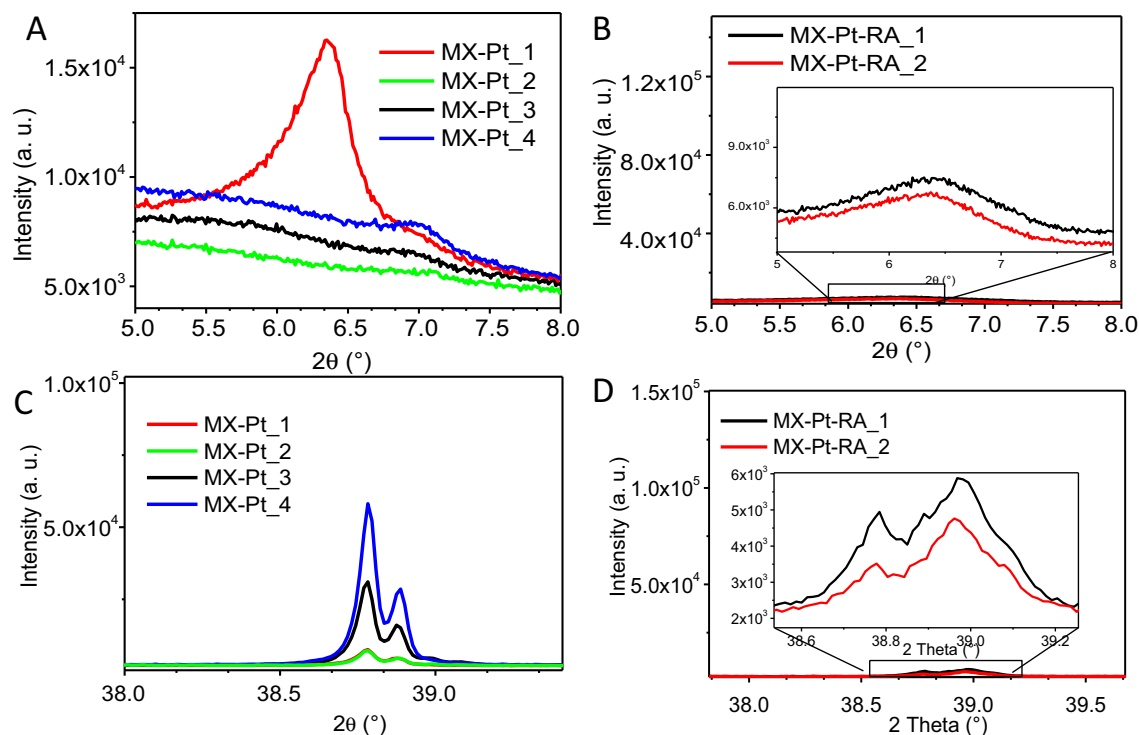
Figure 2. XRD pattern of (A, B) MXene (2θ of approximately 9.5°) and (C, D) Pt (2θ of approximately 38.8–39°) observed in samples prepared without (A, C) and with (B, D) the reducing agent.

be noted that according to Bragg's law, the calculated lattice parameter of the formed crystallites, i.e., distance between two adjacent layers of atoms in the lowest level of order, was very similar for all samples. It was approximately 1.320 ± 0.060 and 0.928 ± 0.001 nm for the first and second MXene peaks, respectively, and 0.232 and 0.228 nm for the first and second Pt peaks, respectively.

XPS analysis was used to further elucidate the structural changes of the MXene structure in its respected PtNPs/MXene composition. For all samples, the XPS peaks for the main expected components, i.e., C, O, Ti, F and Pt, were detected. High-resolution spectra with relevant fitting curves are depicted in Fig. 3 and Fig. S2.

C:.—Upon the synthesis of PtNPs without the RA, the main C1 s peak (binding energy 284.7 eV, assigned to C-C bonds[49]) was found to decrease. For the samples prepared with the RA, on the other hand, the major process was a substantial decrease in the peak at approx. 289 eV assigned to surface-adsorbed COO[49,50] after an increase of the incubation time with RA from 5 to 24 hours, and the C-C peaks could no longer be observed. This may suggest, in accordance with EDX analysis (Fig. S1) that, without the RA, the surface becomes densely covered with a Pt "layer" shielding the MXene substrate (since the penetration of radiation during XPS is very low). Interestingly, only samples with the supposed highest Pt amount (MX-Pt_4 and MX-Pt-RA_2) exhibited small peaks at 281.7 and 282 eV, respectively, assigned to C-Ti-Tx where Tx represents –OH, -F or =O groups.[51] This observation can be associated with some structural changes in the initial material caused by growth of Pt nanoparticles or their clusters.

Ti:.—No samples exhibited peaks assigned to Ti-C (455 eV[51]). For samples prepared without the RA the most significant component was the TiO₂ peak at 458.6 (458.4 for MXPt_3) eV – see Fig. 3A. It should be noted that the detected Ti⁴⁺ appears as a doublet with a peak separation of 5.7 eV,[32] which could also be observed in our samples (Fig. 3A). MX-Pt_4 not only exhibited the TiO₂ component but also a peak at 456.4 eV, which can be most likely related to a "reduced charged state" (or sub-stoichiometric) TiO₂.[32,51] Interestingly, this component

was identified also in the MX-Pt-RA_2 sample, but not in its counterpart prepared with shorter incubation. After relating the fitted peak areas to the sum of all detected areas for the individual samples, it was revealed that for MX-Pt_1 and MX-Pt_3, the measured Ti content was 4.6 and 4.7%, respectively, while for MX-Pt_4 it was 44.6%. For the RA samples, the peak at 459.7 eV was observed, which can be assigned to TiO₂-x-Fx[51] instead of "pure" TiO₂ (Fig. 3B). Furthermore, the MX-Pt-RA_2 sample also exhibited a small peak at 456.2 eV, assigned to Ti³⁺ and/or Ti²⁺, i.e., titanium in "a reduced" state.[52]

Pt:.—All samples exhibited peaks of Pt 4f7/2 and Pt 4f5/2[53] (see Figs. 3C, 3D). From Table S2 an interesting trend can be seen, i.e., a shift of the binding energy of approximately 2 eV to lower values for MX-Pt_4 relative to other samples prepared without the RA. This indicates that the PtNPs for sample MX-Pt_4 enhance the electron transfer from the support,[54,55] and the interaction of the Pt NPs with Ti₃C₂Tₓ is more pronounced. On the other side, the samples prepared with the RA (Fig. 3D) have had their Pt peaks shifted oppositely, approximately 1 eV higher than MX-Pt_1 and MX-Pt_2. These shifts are most likely a result of divergence from the zero-valence state of Pt caused by the possible interaction with electronegative moieties on the substrate MXene surface.[53] It can then be concluded that samples prepared with the RA contain a higher portion of non-zero valent Pt resulting from the higher Ti oxidation level.

Catalytic properties.—CV on stationary electrodes.—In the first series of experiments the MX-Pt samples prepared without the reducing agent were tested for their ORR capability. The MX-Pt dispersions were deposited on disk GCE electrodes and dried under reduced pressure, and the CVs of such electrodes in 100 mM NaOH were performed (see results in Fig. 4A). These experiments revealed that a 5% concentration of the Pt precursor led to a slightly higher ORR rate compared to the original Ti₃C₂Tₓ sample (catalytic current density of 597 ± 3 μA cm⁻²). While the largest current density of ORR was, as expected, achieved with the MX-Pt_4 sample (800 ± 113 μA cm⁻²), all other MX-Pt samples exhibited approximately 20% lower values
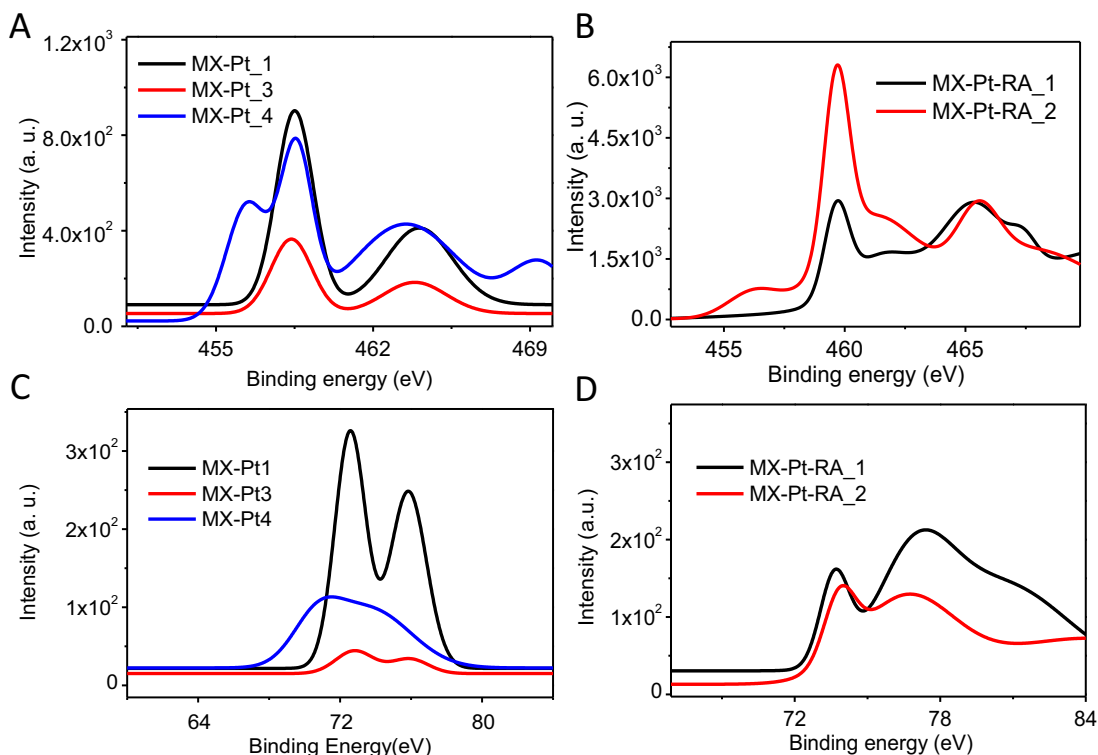
Figure 3. High-resolution XPS Ti2p (A, B) and Pt4f (C, D) spectra of MX-Pt_1, MX-Pt_3 and MX-Pt_4 (A, C) and MX-Pt-RA_1 and MX-Pt-RA_2 (B, D).

(all current values were read at 36 mV vs. RHE from the cathodic parts on the background-corrected CVs; see Fig. 4A). Because of the limited diffusion of dissolved oxygen in an aqueous electrolyte, the obtained maximum current densities will provide rather preliminary information. The more important result here is that both samples with 25% Pt precursor exhibited a decrease in the ORR overpotential (ORR onset was observed at approximately 850 mV (vs. RHE) compared to an onset at 710 mV (vs. RHE) observed for $Ti_3C_2T_X$, MX-Pt_2 and MX-Pt_1). Furthermore, the observed pattern of the ORR electrocatalysis for $Ti_3C_2T_X$ MXene in aerated NaOH without rotation of the modified electrode was consistent with results reported previously.[33]

In the next step, the hydrogen evolution reaction (HER reaction) capability of the MX-Pt samples was tested using CVs performed in 100 mM deaerated H_2SO_4, with results shown in Fig. 4B. A more significant influence of the PtNP amount than in a case of ORR was observed. While a relatively low reduction current density was ob-

served for $Ti_3C_2T_X$ (approximately 1 mA cm^{-2}), the MX-Pt_2 and MX-Pt_1 samples exhibited maximum current densities of -26.5 ± 4.6 and -31.5 ± 2.3 mA cm^{-2}, respectively (measured at -745 mV), with onset potentials at approximately -220 and -150 mV. As expected, the MX-Pt_3 and MX-Pt_4 samples exhibited even larger HER current densities, i.e., 41.0 ± 12.0 and 76.3 ± 13.7 mA cm^{-2}, respectively. It should be noted that the same behavior was observed also at physically more relevant potential (from approximately -250 mV vs. RHE). Additionally, the onset potential was shifted further to more positive values up to approximately -40 and 0 mV for the MX-Pt_3 and MX-Pt_4 samples, respectively. These results indicate that the initial concentration of Pt precursor is more important parameter than the incubation time.

Here, the correlation between the electrocatalytic activity and the amount of the synthesized PtNPs in the MX-Pt composites should be questioned. Even though the samples prepared with 14% of Pt
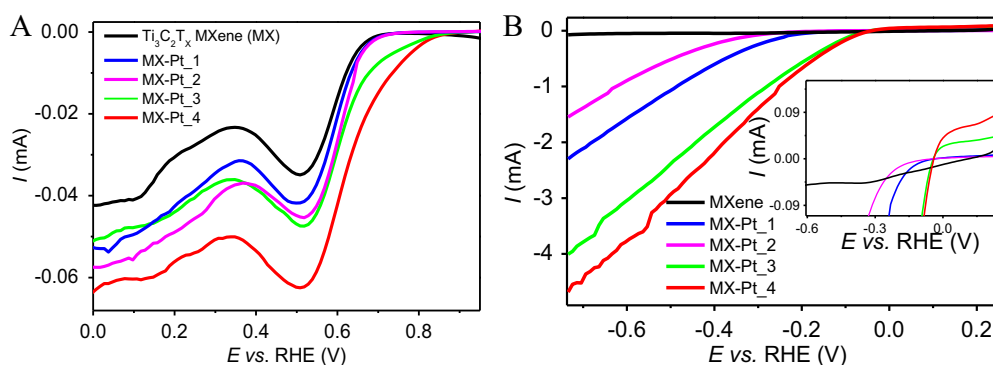
Figure 4. (A) Blank-corrected potentiodynamic polarization curves of GCEs modified with $Ti_3C_2T_X$ (black), MX-Pt_4 (red), MX-Pt_3 (green), MX-Pt_1 (blue) and MX-Pt_2 (cyan) on cathodic part. (B) Potentiodynamic polarization curves obtained with GCEs modified with $Ti_3C_2T_X$ MXene (black), MX-Pt_4 (red), MX-Pt_3 (green), MX-Pt_1 (blue) and MX-Pt_2 (cyan) on anodic part. Inset is enlarged part of the graph to show better the electrocatalytic curve of the MXene without Pt in comparison to other samples. Measured in (A) O_2-bubbled 100 mM NaOH and (B) deaerated 100 mM H_2SO_4. Potential E is vs. RHE electrode.

precursor concentration exhibited a remarkably lower overpotential and higher current density compared to MX-Pt_1 and MX-Pt_2, the EDX results did not confirm that MX-Pt_3 contained a significantly higher concentration of Pt than MX-Pt_1 and MX-Pt_2. Furthermore, MX-Pt_4 contains approximately 5-fold more Pt than MX-Pt_3, but their overpotentials do not differ significantly, nor do their achieved current densities. These facts illustrated the limitations existing under the given experimental conditions, most likely constituted by the limited mass and/or charge diffusion.

In further experiments, by employing rotating disc electrodes, only the samples with the lowest and highest amount of PtNPs (i.e., MX-Pt_1 and MX-Pt_4, respectively) have been used and compared with samples prepared with an external reducing agent (i.e., MX-Pt-RA_1 and MX-Pt-RA_2).

RDE experiments.—To gain further insight into the kinetics and mechanism of the observed reactions, CV experiments were performed with a total of 10 μg of MX, MX-Pt_1, MX-Pt-RA_1, MX-Pt_4 and MX-Pt-RA_2 dispersions deposited on the surface of a 0.196 cm² rotating disk glassy carbon electrode (GCE RDE) at different rotation rates. CVs were performed in both aerated and deaerated 100 mM NaOH and 100 mM H₂SO₄.

ORR.—First, without a background correction, current densities exceeding 2 mA cm⁻² were achieved for all samples in oxygen-saturated 100 mM NaOH, at a rotation rate of 2 000 rpm and a potential of −50 mV (vs. RHE). Under these conditions, however, the unmodified GCE rotation disc electrode exhibited a current density of −2.5 ± 0.3 mA cm⁻², which was very close to the values obtained with all other samples. From these values it is also obvious that there is, in fact, only a very small increase in the catalytic current density after modification of Ti₃C₂Tₓ with Pt nanoparticles. The most likely reason for the small increase is that the Pt amount is simply not high enough to perform efficient oxygen reduction. It was mentioned earlier that common Pt-C catalysts used for oxygen reduction contain at least tenfold more Pt than our samples. It should also be noted that repeating these experiments under acidic conditions (i.e., in 100 mM H₂SO₄) did not generate satisfactory results; none of the samples exhibited significantly higher background-corrected densities than did the non-modified RDE.

HER.—While certain limitations hindered the ORR on MX-Pt hybrids, undoubtedly, both MX and MX-Pt nanoparticles have significantly increased HER reduction currents (see Fig. 5 and Table II). Maximum current densities (read at potential of −745 mV vs. RHE) of 4.3 ± 3.6, 16.7 ± 1.6 (relatively similar to Ref. 24), 61.4 ± 1.7 and 61.9 ± 9.9 mA cm⁻² were observed for unmodified, MX-, MX-Pt-RA_1- and MX-Pt-RA_2-modified electrodes, respectively. This significant increase in the current generation was accompanied by a shift of the reaction onset potential from −570 mV detected with unmodified RDE to −140 mV with MX-Pt-RA_2. Interestingly, different Pt content on electrodes (Table I) had no significant influence on HER efficiency. To explain this, HER catalytic inefficiency of certain portion of the synthesized PtNP can be considered. Detailed analysis of this effect is, however, beyond the scope of this work.

Without the reducing agent, even higher current densities were observed (at −745 mV vs. RHE), namely, 58.0 ± 2.0 and 86.0 ±
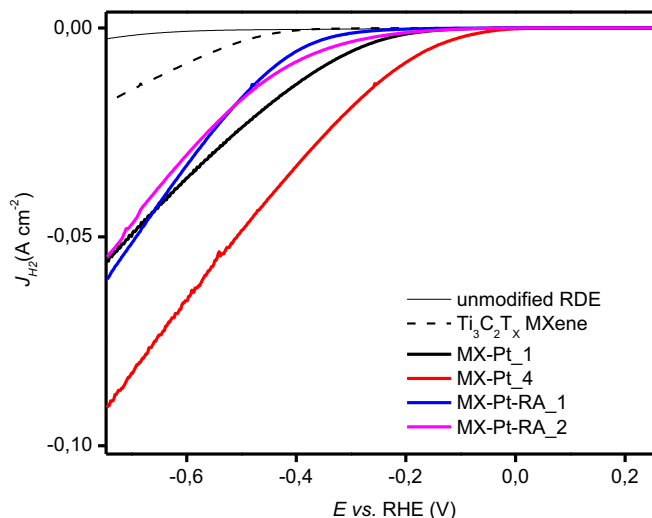
Figure 5. Potentiodynamic polarization curves performed in deaerated 100 mM H₂SO₄, at 2 000 rpm rotation speed with unmodified RDE (thin black), MX-, MX-Pt_1-, MX-Pt_4-, MX-Pt-RA_1-, MX-Pt-RA_2- modified RDEs.

6.0 mA cm⁻² for MX-Pt_1- and MX-Pt_4-modified RDEs, respectively. It was observed that without the reducing agents, the catalytic performances were significantly improved not only at the above-mentioned potential which is of low relevance when it comes to real applications (fuel cells, electrolysis cells...), but also at −250 mV, i.e. much usable potential. The same is valid for all samples.

The observed differences in the HER catalytic current density were accompanied by shifts in the reduction onset potential toward more positive values, i.e., an overpotential decrease for more catalytically active nanohybrids. Values of the measured reduction onset potentials as well as potentials at which the catalytic current density of 10 mA cm⁻² (E_{jl0}) was observed are listed in Table II. In addition to the observed HER activity enhancement of the MXene samples modified with PtNPs, it can be further concluded that this activity is at its maximum when the modification is performed without the additional reducing agent and when the reaction time and initial Pt precursor concentrations are the highest, e.g., sample MX-Pt_4.

Coy et al. reported NbC prepared by sputter-deposition, which exhibited an onset potential of −161 mV vs. RHE and approximately −380 mV potential at a 10 mA cm⁻² current density.[56] These values confirmed that titanium carbide-based materials with originally lower HER catalytic activity can significantly improve by the in situ reduction deposition of PtNPs. Importantly, material characteristics suggests that the Pt amount needed to convert titanium carbide MXene[24] into an HER catalyst that outperforms Pt-like Nb carbide is several times lower than the amount used in most conventional PtNP-based nanocatalysts. As a matter of fact, RDE modified with MX-Pt_4 provided approximately 60.3 mA cm⁻² by 1 μg of Pt (as calculated from values in Table I and Table II). Interestingly, samples prepared with the RA provided even 5- and 11- fold larger catalytic current density per 1 μg of Pt, which should suggest better electrocatalytic performance. On the other side, larger overpotentials for MX-Pt-RA samples compared to MX-Pt_1 and _4 suggest that

Table II. Measured values of potentials where catalytic current density in deaerated buffer of 10 mA cm⁻² was reached (E_{jl0}), potentials of onset of HER reduction, HER current densities at −745 mV vs. RHE (j_{H2}) and catalytic currents resulted from subtraction of CVs measured in the deaerated H₂SO₄ from the ones measured in the air-saturated one (j_{O2}).

| Electrode	E_{jl0} (mV vs. RHE)	Onset potential (mV vs. RHE)	j_{H2} (mA cm⁻²)	j_{O2} (mA cm⁻²)
RDE	......	−570 ± 25	−4 ± 4	−8 ± 5
MX	−651 ± 24	−379 ±43	−17 ± 1	−13 ± 6
MX-Pt_1	−355 ± 13	−153 ± 3	−58 ± 3	−4 ± 0
MX-Pt_4	−226 ± 9	−76 ± 5	−87 ± 6	−8
MX-Pt-RA_1	−434 ± 21	−214 ± 28	−61 ± 2	−9 ± 1
MX-Pt-RA_2	−416 ± 15	−148 ± 31	−62 ± 10	−6
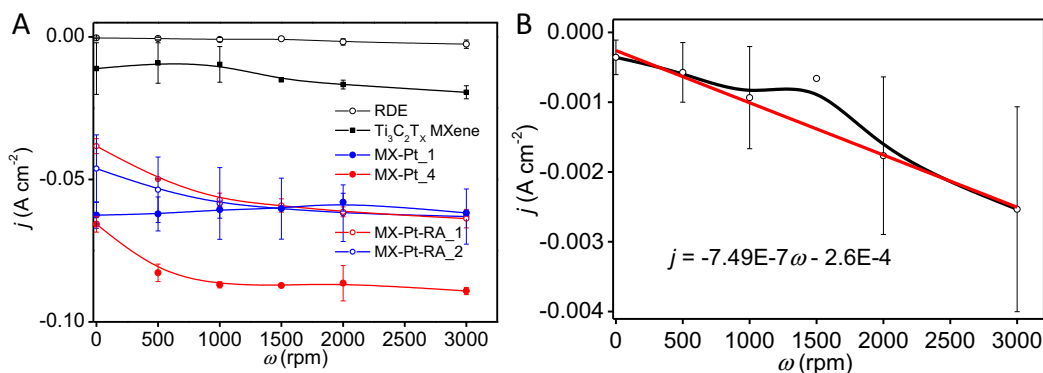
Figure 6. (A) Dependence of current density j vs. rotation rate ω for unmodified RDE (black circles), MX- (black squares), MX-Pt-RA_1-, MX-Pt-RA_2- (red and blue circles, respectively), MX-Pt_1- and MX-Pt_4- modified electrodes (red and blue dots, respectively) in deaerated 100 mM H_2SO_4. Values were read at −745 mV vs. RHE. Inserted B-spline lines are only guides for eyes. (B) Detail of the j-ω dependence of unmodified RDE, with linear fit (red line).

the opposite is true, most probably because of inefficient mass/charge diffusion through the "ballast" original MXene substrate. It is than reasonable to conclude that not only Pt amount but also the structure of the electrocatalytic nanomaterial (or any other parameter influencing mass/charge exchange) is what really matters.

Another qualitative parameter is a dependence of the reduction current on the rotation rate (j-ω plot). From Fig. 6 it can be concluded that the current density (read at −745 mV vs. RHE) provided by the sample with the lowest Pt amount, i.e., MX-Pt-RA_1, exhibited negligible dependence on the rotation rate. All other samples exhibited an initial increase in the current with the increased rotation rate, which reached a plateau after approximately 1 500 rpm. It can be concluded that at that point, the electrocatalysis rate became a limiting factor in determining the power density level, and the increased mass diffusion (the positive effect of the increased rotation rate) could no longer be observed. Hence, from the lack of dependence j-ω at RDE modified with MX-Pt-RA_1, it can be inferred that this material provided a much slower HER rate. In other words, the reaction-based limitations were much more severe than in other samples. It should also be noted that this behavior is similar to the observed j-ω dependence of unmodified MXene, even though in this case the obtained data were more ambiguous. Fig. 6B also shows that the unmodified RDE exhibited almost ideally linear j-ω dependence over the entire rotation rate range with a slope of -7.485×10^{-7}, which is much smaller than the slopes of the j-ω functions measured in the quasi-table plateau (1 000–3 000 rpm) for MX-Pt_4 (slope of -1.1×10^{-6}), MX-Pt-RA_2 (slope of -2.3×10^{-6}), MX-Pt-RA_1 (slope of -3.3×10^{-6}) and MX (slope of -4.9×10^{-6}). From these results it can be concluded that all samples enhanced the heterogeneous surface HER rate.

The nature of the achieved HER reaction can also be determined by the measurement of the Tafel slopes calculated as the slope of the log j vs. η curve. It is stated that the slope of 30 mV dec^{-1} is assigned to the HER where the desorption step $H_{ads} + H_{ads} \rightarrow H_2$ is rate-limiting in the overall $2H^+ + 2e^- \rightarrow H_2$ HER reaction. Furthermore, the maximum slope of 120 mV dec^{-1} is typical for processes with a bottle-neck represented by the "Volmer discharge" reaction $H_3O^+ + e^- \rightarrow H_{ads} + H_2O$.[57] The measurement of RDE/MX-Pt-4 in the deaerated 100 mM H_2SO_4 at 1 600 rpm revealed a Tafel slope of 59.54 ± 0.34 mV dec^{-1} (Fig. 7A), which is lower than for Ti_2CT_X (124–169 mV dec^{-1}) and Mo_2CT_X (70-82 mV dec^{-1}) reported elsewhere.[24] On the other side the Tafel slope is larger than the best-performing HER-catalysing nanomaterials, e.g., the standard Pt/C catalyst (30 mV per decade with dependence on operational conditions, see e.g., Ref. 57 and references therein) or N-doped graphene decorated by Pt-Pd alloy nanoparticles (32 mV per decade; different fabrication conditions, however, offered Tafel slopes of 60–95 mV dec^{-1} Ref. 58) and larger than results achieved on MoS_2-deposited mesoporous graphene foam (42 mV dec^{-159}), coupled Mo carbide and reduced graphene oxide nanocatalysts (34 mV dec^{-160}) or other transition metal carbides (NbC 35 mV dec^{-156}). In fact, our results are closer to values typical for best-performing non-metallic HER nanocatalysts, e.g., graphene coated with nanoribbons of graphitic carbon nitride (54 mV dec^{-161} or 51 mV dec^{-162}), carbonized and cathodically activated bacterial mass (58 mV dec^{-163}) or carbonized and N-doped bacterial cellulose integrated with MoS_2 (61 mV dec^{-164}). MoS_2 nanocatalysts could provide a low Tafel slope of 55 mV dec^{-1}, but only under some special conditions.[65]
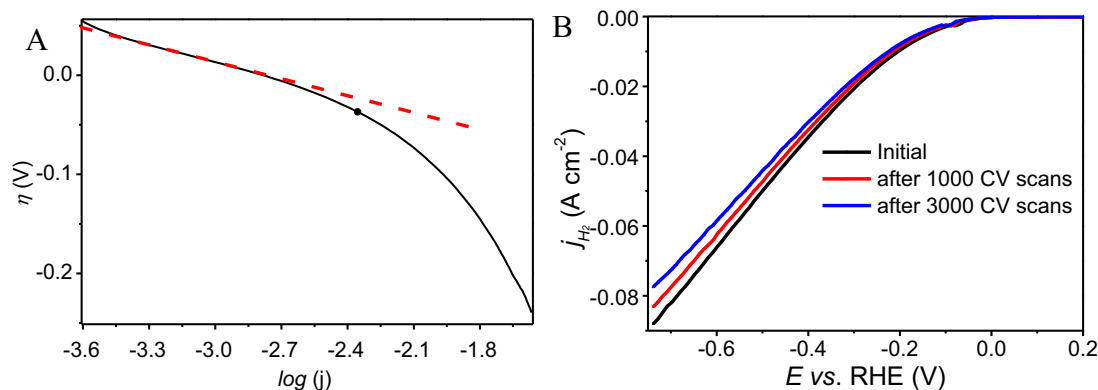
Figure 7. (A) Tafel slope (red line) measured at MX-Pt_4-modified RDE at 2 000 rpm in 100 mM deaerated H_2SO_4 – obtained semilogarithmic voltammogram is the black curve. (B) Polarization curves of MX-Pt_4 after initial run (black), 1 000 (red) and 3 000 cycles (blue) in deaerated 100 mM H_2SO_4 solution at 2 000 rpm, respectively.

Hence, it can be concluded that the MX-Pt_4 surface HER dynamics slightly differ from the one observed on pure Pt/C nanocatalysts.

The operational stability of electrodes modified by the best-performing material was also examined. The ability of these electrodes (i.e., RDE/MX-Pt_4) to undergo multiple consecutive CVs was measured at 2 000 rpm in a deaerated 100 mM H_2SO_4 solution for 3 000 CV scans at a scan rate of 50 mV s^{-1}. As shown in Fig. 7B, the activity after 3 000 cycles showed negligible change in the onset potential compared to that in the initial cycle. A slight decrease was observed at 95 and 88% of the initial maximum current density (at −745 mV vs. RHE) after 1 000 and 3 000 scans, respectively. The hydrogen evolution rate drop can be attributed either to lower diffusion rate of the hydrogen evolved in the HER process resulting from some chemical changes on the surface (electrode fouling) or, more probably, by a slow displacement of the catalytic material from the electrode surface. For example, Xie et al. reported enhanced electrochemical stability of the MX-Pt composite compared to a conventional Pt/C catalyst as well as a decrease of ca. 16% in the electrochemically active area after 10 000 CV cycles in aerated $HClO_4$.[27] On the other side, MX-Pt did not exhibit any significant shift in the onset potential of the HER, which is unlike the onset shifts observed, e.g., at Ti_2CT_X MXene[24] or natural cellulose-derived N, P and S-doped carbon HER catalyst.[66] XRD measurements performed on the electrode after electrolysis (3 000 cycles), clearly shows the presence of both the MXene and Pt phases, as seen in Fig. S3, thus making MX-Pt an attractive HER catalyst. Notably, regardless of the insubstantial decrease in HER activity with successive CV scanning, sufficient stability of this coating was achieved even without the use of a binder, such as Nafion.

Conclusions

Substantial differences were observed in the structure and composition of PtNPs synthesized in situ on a $Ti_3C_2T_X$ MXene surface. XRD, SEM, EDX mapping and XPS characterizations revealed that when additional reducing agent $NaBH_4$ was used, Pt nanoparticles stacked approximately into clusters, and the initial $Ti_3C_2T_X$ MXene remained relatively unchanged after PtNPs synthesis. Furthermore, without $NaBH_4$, the Pt precursor was more intensively reduced by the initial MXene particles, which, in turn, changed the MXene nanoparticle structure. This method provided a nanohybrid with a higher overall concentration of Pt, and the observed PtNPs formed composites assembled into larger clusters, while individual nanoparticles exhibited approximate diameters of 3 nm. The differences in the synthesized NPs together with presumed changes in the initial MXene substrate structure induced by the synthesis process are shown in the observed electrocatalytic properties. While the ORR rate of the prepared samples was not sufficiently higher, it has the potential to be enhanced by the increased amount of catalyst on the electrode surface and/or by the application of the hydrophobic polymer matrix. This assumption was made according to the fact that the EDX revealed lower Pt content in the MX-Pt samples than was reported for most commonly used Pt/C ORR catalysts, which is another factor playing a role in the insufficient rate of the ORR observed. Moreover, a great increase in HER was observed after the modification of MXene with PtNPs. Interestingly, samples MX-Pt provided a significantly higher current density without RA than with RA, which can be ascribed to a higher PtNPs amount; however, in both samples prepared with the RA reduction, the amount of the PtNPs is significantly different, but the obtained HER currents are relatively similar. Furthermore, dependence of the obtained current densities on the electrode rotation rate was investigated, and the results have supported the enhanced HER rate on the MXene samples modified with PtNPs, excluding the sample with a lowest Pt concentration. The MX-Pt_4 sample exhibiting the highest HER activity was further tested for its long-term operational stability under a 2 000 rpm rotation condition with a 5 and 12% drop in the maximum current density observed after the 1 000 and 3 000 CV scans, respectively. Notably, this stability was achieved without any additional binder, i.e., Nafion or PTFE. The nature of the observed HER reaction was also tested calculating the Tafel slopes from the polarization curves. The MX-Pt_4 sample provided a higher Tafel slope than the "pure" Pt/C HER nanocatalyst, but the achieved values (slightly below 60 mV dec^{-1}) suggested a better performance than typical non-metal HER catalysts, including heteroatom-doped graphene and molybdenum di- and trisulfide-based nanocatalysts. In summary, this work illustrates the influence of the preparation conditions on the electrocatalytic performance of HER nanocatalysts consisting of in situ synthesized Pt nanoparticles on $Ti_3C_2T_X$ MXene nanosheets. It was found that quite counterintuitively, spontaneous reduction led to the preparation of more efficient catalysts. It can also be concluded that the oxidation of initial MXene nanoparticles (especially embedded Ti atoms) associated with the reduction of Pt ions and formation of Pt nanoparticles provided MX-Pt nanocatalysts with better growth of PtNPs compared to when the reduction of Pt ions by $NaBH_4$ occurs in solution, and the $Ti_3C_2T_X$ structure is mostly retained.

ORCID

Peter Kasak 🔶 https://orcid.org/0000-0003-4557-1408

References

1. M. Chhowalla, H. S. Shin, G. Eda, L.-J. Li, K. P. Loh, and H. Zhang, *Nature Chemistry*, **5**, 263 (2013).
2. D. Merki and X. Hu, *Energy & Environmental Science*, **4**, 3878 (2011).
3. L. Yang, C. Xie, J. Jin, R. Ali, C. Feng, P. Liu, and B. Xiang, *Nanomaterials*, **8**, 463 (2018).
4. T. H. M. Lau, X. Lu, J. Kulhavý, S. Wu, L. Lu, T.-S. Wu, R. Kato, J. S. Foord, Y.-L. Soo, K. Suenaga, and S. C. E. Tsang, *Chemical Science*, **9**, 4769 (2018).
5. J. Bai, S.-H. Xing, Y.-Y. Zhu, J.-X. Jiang, J.-H. Zeng, and Y. Chen, *Journal of Power Sources*, **385**, 32 (2018).
6. D. K. Singh, R. N. Jenjeti, S. Sampath, and M. Eswaramoorthy, *Journal of Materials Chemistry A*, **5**, 6025 (2017).
7. W. Cui, Q. Liu, N. Cheng, A. M. Asiri, and X. Sun, *Chemical Communications*, **50**, 9340 (2014).
8. J. Zhang, L. Qu, G. Shi, J. Liu, J. Chen, and L. Dai, *Angewandte Chemie International Edition*, **55**, 2230 (2016).
9. H. V. Le, Q. T. T. Nguyen, T. T. Co, P. K. T. Nguyen, and H. T. Nguyen, *Journal of Electronic Materials*, **47**, 6918 (2018).
10. Q. Wang, M. Ming, S. Niu, Y. Zhang, G. Fan, and J.-S. Hu, *Advanced Energy Materials*, **8**, 1801698 (2018).
11. X. Yan, H. Li, J. Sun, P. Liu, H. Zhang, B. Xu, and J. Guo, *Carbon*, **137**, 405 (2018).
12. D. Hu, Y. Shi, Y. Du, W. Yu, J. Huang, H. Gao, and M. Zhu, *Polymer*, **153**, 331 (2018).
13. J. M. M. Tengco, B. A. Tavakoli Mehrabadi, Y. Zhang, A. Wongkaew, J. R. Regalbuto, J. W. Weidner, and J. R. Monnier, *Catalysts*, **6**, 83 (2016).
14. J.-Y. Lee, W.-K. Lee, H.-R. Rim, G.-B. Joung, J. W. Weidner, and H.-K. Lee, *Journal of Nanoscience and Nanotechnology*, **16**, 6383 (2016).
15. J. Chen, B. Lim, E. P. Lee, and Y. Xia, *Nano Today*, **4**, 81 (2009).
16. W. Sheng, H. A. Gasteiger, and Y. Shao-Horn, *Journal of The Electrochemical Society*, **157**, B1529 (2010).
17. M. Naguib, O. Mashtalir, J. Carle, V. Presser, J. Lu, L. Hultman, Y. Gogotsi, and M. W. Barsoum, *ACS Nano*, **6**, 1322 (2012).
18. V. M. Hong Ng, H. Huang, K. Zhou, P. S. Lee, W. Que, J. Z. Xu, and L. B. Kong, *Journal of Materials Chemistry A*, **5**, 3039 (2017).
19. Z. Ling, C. E. Ren, M.-Q. Zhao, J. Yang, J. M. Giammarco, J. Qiu, M. W. Barsoum, and Y. Gogotsi, *Proceedings of the National Academy of Sciences*, **111**, 16676 (2014).
20. M. Naguib, J. Come, B. Dyatkin, V. Presser, P.-L. Taberna, P. Simon, M. W. Barsoum, and Y. Gogotsi, *Electrochemistry Communications*, **16**, 61 (2012).
21. X. Zhu, B. Liu, H. Hou, Z. Huang, K. M. Zeinu, L. Huang, X. Yuan, D. Guo, J. Hu, and J. Yang, *Electrochimica Acta*, **248**, 46 (2017).
22. X.-F. Yu, Y.-C. Li, J.-B. Cheng, Z.-B. Liu, Q.-Z. Li, W.-Z. Li, X. Yang, and B. Xiao, *ACS Applied Materials & Interfaces*, **7**, 13707 (2015).
23. F. Wang, C. Yang, C. Duan, D. Xiao, Y. Tang, and J. Zhu, *Journal of The Electrochemical Society*, **162**, B16 (2015).
24. Z. W. Seh, K. D. Fredrickson, B. Anasori, J. Kibsgaard, A. L. Strickler, M. R. Lukatskaya, Y. Gogotsi, T. F. Jaramillo, and A. Vojvodic, *ACS Energy Letters*, **1**, 589 (2016).
25. L. Lorencova, T. Bertok, J. Filip, M. Jerigova, D. Velic, P. Kasak, K. A. Mahmoud, and J. Tkac, *Sensors and Actuators B: Chemical*, **263**, 360 (2018).

26. E. Satheeshkumar, T. Makaryan, A. Melikyan, H. Minassian, Y. Gogotsi, and M. Yoshimura, *Scientific Reports*, **6**, 32049 (2016).
27. X. Xie, S. Chen, W. Ding, Y. Nie, and Z. Wei, *Chemical Communications*, **49**, 10112 (2013).
28. W. Li, C. Liang, W. Zhou, J. Qiu, G. Sun, and Q. Xin, *J Phys Chem B*, **107**, 6292 (2003).
29. X. Xie, Y. Xue, L. Li, S. Chen, Y. Nie, W. Ding, and Z. Wei, *Nanoscale*, **6**, 11035 (2014).
30. L. Su, W. Jia, C.-M. Li, and Y. Lei, *ChemSusChem*, **7**, 361 (2014).
31. R. Singh, R. Awasthi, and C. Sharma, *Int. J. Electrochem. Sci*, **9**, 5607 (2014).
32. B. Ahmed, D. H. Anjum, M. N. Hedhili, Y. Gogotsi, and H. N. Alshareef, *Nanoscale*, **8**, 7580 (2016).
33. L. Lorencova, T. Bertok, E. Dosekova, A. Holazova, D. Paprckova, A. Vikartovska, V. Sasinkova, J. Filip, P. Kasak, M. Jerigova, D. Velic, K. A. Mahmoud, and J. Tkac, *Electrochimica Acta*, **235**, 471 (2017).
34. M. Taleb, J. Nerut, T. Tooming, T. Thomberg, and E. Lust, *Journal of The Electrochemical Society*, **163**, F1251 (2016).
35. M. Kim, J.-N. Park, H. Kim, S. Song, and W.-H. Lee, *Journal of Power Sources*, **163**, 93 (2006).
36. R. P. Pandey, K. Rasool, V. E. Madhavan, B. Aïssa, Y. Gogotsi, and K. A. Mahmoud, *Journal of Materials Chemistry A*, **6**, 3522 (2018).
37. J. Wang, J. Yu, X. Zhu, and X. Z. Kong, *Nanoscale Research Letters*, **7**, 646 (2012).
38. K. Sakurai and M. Mizusawa, *Analytical Chemistry*, **82**, 3519 (2010).
39. R. L. Franco, T. G. Oliveira, A. M. G. Pedrosa, S. Naviciene, and M. J. Souza, *Materials Research*, **16**, 1448 (2013).
40. L. Biasetto, H. Elsayed, F. Bonollo, and P. Colombo, *Surface and Coatings Technology*, **301**, 140 (2016).
41. S. Andersson, B. Collén, U. Kuylenstierna, and A. Magnéli, *ActaChemicaScandinavica*, **11**, 1641 (1957).
42. S. Harada, K. Tanaka, and H. Inui, *Journal of Applied Physics*, **108**, 083703 (2010).
43. S.-I. Ohkoshi, Y. Tsunobuchi, T. Matsuda, K. Hashimoto, A. Namai, F. Hakoe, and H. Tokoro,, *Nature Chemistry*, **2**, 539 (2010).
44. T. Ioroi, T. Akita, S.-I. Yamazaki, Z. Siroma, and N. K. Fujiwara, Yasuda, *Journal of The Electrochemical Society*, **158**, C329 (2011).
45. T. Ioroi, Z. Siroma, N. Fujiwara, S.-I. Yamazaki, and K. Yasuda, *Electrochemistry Communications*, **7**, 183 (2005).
46. A. Kaniyoor, R. Imran Jafri, T. Arockiadoss, and S. Ramaprabhu, *Nanoscale*, **1**, 382 (2009).
47. Y. Wang, J. Liu, L. Liu, and D. D. Sun, *Nanoscale Research Letters*, **6**, 241 (2011).
48. D. He, Y. Rong, Z. Kou, S. Mu, T. Peng, R. Malpass-Evans, M. Carta, N. B. McKeown, and F. Marken, *Electrochemistry Communications*, **59**, 72 (2015).
49. S. A. Shah, T. Habib, H. Gao, P. Gao, W. Sun, M. J. Green, and M. Radovic, *Chemical Communications*, **53**, 400 (2017).
50. P. Jayaweera, E. Quah, and H. Idriss, *The Journal of Physical Chemistry C*, **111**, 1764 (2007).
51. J. Halim, K. M. Cook, M. Naguib, P. Eklund, Y. Gogotsi, J. Rosen, and M. W. Barsoum, *Applied Surface Science*, **362**, 406 (2016).
52. S. Yamamoto, H. Bluhm, K. Andersson, G. Ketteler, H. Ogasawara, M. Salmeron, and A. Nilsson, *Journal of Physics: Condensed Matter*, **20**, 184025 (2008).
53. G. Fan, X. Li, Y. Ma, Y. Zhang, J. Wu, B. Xu, T. Sun, D. Gao, and J. Bi, *New Journal of Chemistry*, **41**, 2793 (2017).
54. L. Qiu, F. Liu, L. Zhao, W. Yang, and J. Yao, *Langmuir*, **22**, 4480 (2006).
55. Q. Tang, Z. Zhou, and P. Shen, *Journal of the American Chemical Society*, **134**, 16909 (2012).
56. E. Coy, L. Yate, D. P. Valencia, W. Aperador, K. Siuzdak, P. Torruella, E. Azanza, S. Estrade, I. Iatsunskyi, F. Peiro, X. Zhang, J. Tejada, and R. F. Ziolo, *ACS Applied Materials & Interfaces*, **9**, 30872 (2017).
57. T. Shinagawa, A. T. Garcia-Esparza, and K. Takanabe, *Scientific Reports*, **5**, 13801 (2015).
58. X. Zhong, Y. Qin, X. Chen, W. Xu, G. Zhuang, X. Li, and J. Wang, *Carbon*, **114**, 740 (2017).
59. L. Liao, J. Zhu, X. Bian, L. Zhu, M. D. Scanlon, H. H. Girault, and B. Liu, *Advanced Functional Materials*, **23**, 5326 (2013).
60. J.-S. Li, Y. Wang, C.-H. Liu, S.-L. Li, Y.-G. Wang, L.-Z. Dong, Z.-H. Dai, Y.-F. Li, and Y.-Q. Lan, *Nature Communications*, **7**, 11204 (2016).
61. Y. Zhao, F. Zhao, X. Wang, C. Xu, Z. Zhang, G. Shi, and L. Qu, *Angewandte Chemie International Edition*, **53**, 13934 (2014).
62. Y. Zheng, Y. Jiao, Y. Zhu, L. H. Li, Y. Han, Y. Chen, A. Du, M. Jaroniec, and S. Z. Qiao, *Nature Communications*, **5**, 3783 (2014).
63. L. Wei, H. E. Karahan, K. Goh, W. Jiang, D. Yu, O. Birer, R. Jiang, and Y. Chen, *Journal of Materials Chemistry A*, **3**, 7210 (2015).
64. F. Lai, Y.-E. Miao, Y. Huang, Y. Zhang, and T. Liu, *ACS Applied Materials & Interfaces*, **8**, 3558 (2016).
65. J. Xie, J. Zhang, S. Li, F. Grote, X. Zhang, H. Zhang, R. Wang, Y. Lei, B. Pan, and Y. Xie, *Journal of the American Chemical Society*, **135**, 17881 (2013).
66. A. Mulyadi, Z. Zhang, M. Dutzer, W. Liu, and Y. Deng, *Nano Energy*, **32**, 336 (2017).